Study of Geometrical, Electronic Structure, Spectral and NLO Properties of 6-Amino-2-Methylpyridine (6A2MP) Dye Sensitizer for Solar Cells

P.Sakthivel [a], K.Periyasamy[b],P.M.Anbarasan[C]
a. Department of Physics, Salem Sowdeswari College, Salem -636010,Tamilnadu,India.
b. Department of Physics, A.E.T. College, Attur- 636108,Salem, Tamilnadu, India.
c. Department of Physics, Periyar University,Salem – 636011, Tamilnadu, India.

ABSTRACT

The geometries, electronic structures, polarizabilities, and hyperpolarizabilities of organic dye sensitizer 6A2MP was studied based on ab initio Hartee Fock (HF) and Density Functional Theory (DFT) using the hybrid functional B3LYP. Ultraviolet-visible (UV-Vis) spectrum was investigated by Time Dependent- DFT (TD-DFT). Features of the electronic absorption spectrum in the visible and near-UV regions were assigned based on TDDFT calculations. The absorption bands are assigned to $\pi \rightarrow \pi^*$ transitions. Calculated results suggest that the three excited states with the lowest excited energies in 6A2MP Dye are due to photo induced electron transfer processes. The interfacial electron transfer between semiconductor TiO_2 electrode and dye sensitizer 6A2MP Dye, is due to an electron injection process from excited dye to the semiconductor's conduction band. The role of cyanine and methyl group in 6A2MP Dye in geometries, electronic structures, and spectral properties were analyzed.

1. Introduction

The new technologies for direct solar energy conversion have gained more attention in the last few years. In particular, Dye Sensitized Solar Cells (DSSCs) are promising in terms of efficiency and low cost [1-3]. The foremost feature of DSSC consists in a wide band gap nanocrystalline film grafted with a quasi-monolayer of dye molecules and submerged in a redox electrolyte. This elegant architecture can synchronously address two critical issues of employing organic materials for the photovoltaic applications: (i) efficient charge generation from the Frenkel excitons; (ii) long-lived electron-hole separation up to the millisecond time domain. The latter attribute can often confer an almost quantitative charge collection for several micrometer-thick active layers, even if the electron mobilities in nanostructured semiconducting films are significantly lower than those in the bulk crystalline materials. Benefited from systematic device engineering and continuous material innovation, a state of the art DSSC with a ruthenium sensitizer has achieved a validated efficiency of 11.1% [4] measured under the air mass 1.5 global (AM1.5G) conditions. In view of the limited ruthenium

resource and the heavy-metal toxicity, metal-free organic dyes have received surging research interest in recent years [5-21]. Because of their high molar absorption coefficient, relatively simple synthesis procedure, various structures and lower cost in contrast to a ruthenium dye and the flexibility in molecular tailoring of an organic sensitizer provides a large area to explore [22-24]. Meanwhile, recently a rapid progress of organic dyes has been witnessed reaching close to 10.0% efficiencies in combination with a volatile acetonitrile-based electrolyte [25]. In this Chapter the performance of 6A2MP Dye metal free dye that can be used in DSSC is analyzed.

2. Experimental Details of the 6A2MP

The compound 6A2MP Dye was obtained from Sigma-Aldrich Chemical Company, USA with a stated purity of greater than 99% and it was used as such without further purification. The FT-Raman spectrum of 6A2MP Dye has been recorded using 1064 nm line of Nd: YAG laser as excitation wavelength in the region 50-3500 cm^{-1} on a Brucker model IFS 66 V spectrophotometer. The FT-IR spectrum of this compound was recorded in the region 400-4000 cm^{-1} on IFS 66 V spectrophotometer using KBr pellet technique. The spectrum was recorded at room temperature, with scanning speed of 30 $cm^{-1}min^{-1}$ and the spectral resolution of 2.0 cm^{-1}.

3. Computational Methods

The computations of the geometries, electronic structures, polarizabilities and hyperpolarizabilities, as well as electronic absorption spectrum for dye sensitizer 6A2MP Dye was done using ab initio Hartree Fock (HF) and DFT with Gaussian09w package [26]. The DFT was treated according to Becke's three parameter gradient-corrected exchange potential and the Lee-Yang-Parr gradient-corrected correlation potential (B3LYP) [27–29], and all calculations were performed without any symmetry constraints by using polarized split-valence 6-311++G(d,p) basis sets. The electronic absorption spectrum requires calculation of the allowed excitations and oscillator strengths. These calculations were done using TDDFT with the same basis sets and exchange-correlation functional in vacuum and solution, and the non-equilibrium version of the polarizable continuum model (PCM) [30, 31] was adopted for calculating the solvent effects.

4. Results and Discussion

4.1 The Geometric Structure

The optimized geometry of the 6A2MP Dye is shown in Fig.1.1 and the bond lengths, bond angles and dihedral angles are listed in Table 6.1 Since the crystal structure of the exact title compound is not available till now, the optimized structure can be only be compared with other similar systems for which the crystal structures have been solved. From the theoretical values we can find most of

the optimized bond lengths, bond angles and dihedral angles. The distance between C2 and C3 atoms in cyanine groups of 6A2MP Dye are 1.5037Å and 1.504 Å respectively at B3LYP/6-311++G (d,p) and also compared with HF/6-311++G (d,p).

Fig.6.1 Optimized geometrical structure of dye 6A2MP.

Table 6.1 Bond lengths (in angstrom), bond angles (in degree) and dihedral angles (in degree) of the dye 6A2MP.

Parameters	HF/6-311G(d,p)	DFTB3LYP/6-311G(d,p)
Bond length(Å)		
C1-C2	1.3909	1.4117
C1-N8	1.3247	1.3329
C2-C3	1.5037	1.504
C2-C7	1.4017	1.4057
C3-C4	1.4353	1.4239
C3-N10	1.3627	1.377
C4-C5	1.0751	1.0835
C4-H11	1.4079	1.4102
C5-C6	1.0737	1.0832
C5-H12	1.3179	1.342
C6-C7	1.3613	1.3685
C6-H13	1.1323	1.1573
C7-C9	1.0845	1.0886
C9-H14	1.0809	1.0934
C9-H15	1.0845	1.0943
C9-H16	0.9925	1.0061
N10-H17	0.9939	1.008
Bond Angle(°)		
C1-C2-C3	121.5897	121.5974
C1-C2-C7	122.9247	121.2894
C3-C2-C7	115.4854	117.1132
C2-C3-C4	118.249	118.3576
C2-C3-N10	122.1874	121.0509

C4-C3-N10	119.5636	120.5914
C3-C4-C5	119.9632	119.8046
C3-C4-H11	119.5668	119.6459
C5-C4-H11	120.4699	120.5494
C4-C5-C6	117.5045	118.0009
C4-C5-H12	121.6341	121.1418
C6-C5-H12	120.8599	120.8567
C5-C6-C7	122.6656	122.53
C5-C6-H13	120.7033	121.4795
C7-C6-H13	116.6106	115.9708
C2-C7-C6	120.0271	119.7085
C2-C7-C9	109.1224	109.5538
C6-C7-C9	112.552	111.1318
C7-C9-H14	109.0871	110.7404
C7-C9-H15	109.1586	109.459
C7-C9-H16	107.6451	109.0326
H14-C9-H15	109.1547	106.8643
H14-C9-H16	118.9321	119.9306
H15-C9-H16	116.23	116.6826
C3-N10-H17	116.5929	117.4048
C3-N10-H18	181.2071	179.9478
H17-N10-H18	180.1068	180.0531
Dihedral Angle (°)		
C2-C1-C8-C3-C-1	-0.15	-0.1484
C2-C1-C8-C3-C-2	179.7956	179.7806
C1-C2-C3-C4	-179.9957	179.7983
C1-C2-C3-N10	-0.0501	-0.2727
C7-C2-C3-C4	0.3599	0.3552
C7-C2-C3-N10	-179.7837	-179.5937
C1-C2-C7-C6	121.4889	176.2347
C1-C2-C7-C9	0.1503	55.1514
C3-C2-C7-C6	-121.1588	-63.4643
C3-C2-C7-C9	-58.3655	-3.8163
C2-C3-C4-C5	-179.7041	-124.8996
C2-C3-C4-H11	58.9869	116.4847
N10-C3-C4-C5	-0.1019	-0.1128
N10-C3-C4-H11	-179.9696	179.9535
C2-C3-N10-H17	179.9511	179.9578
C2-C3-N10-H18	0.0834	0.0241
C4-C3-N10-H17	0.1392	0.1596
C4-C3-N10-H18	-179.4178	-179.5609
C3-C4-C5-C6	-179.9943	-179.9074
C3-C4-C5-H12	0.4487	0.3721
H11-C4-C5-C6	0.0701	0.0475
H11-C4-C5-H12	-178.2243	-178.2718
C4-C5-C6-C7	179.6308	179.7688
C4-C5-C6-H13	1.3363	1.4495
H12-C5-C6-C7	-0.3219	-0.3072
H12-C5-C6-H13	178.0379	178.0985

C5-C6-C7-C2	-20.244	-17.4842
C5-C6-C7-C9	-167.6546	-169.0919
H13-C6-C7-C2	161.3619	164.0919
H13-C6-C7-C9	13.9513	11.9934

4.2. Electronic Structures and Charges

Natural Bond Orbital (NBO) analysis was performed in order to analyze the charge populations of the dye 6A2MP Dye. Charge distributions in C, N and H atoms were observed because of the different electro-negativity, the electrons transferred from C atoms to C, N atoms, C atoms to H and N atoms to H atom. The natural charges of different groups are the sum of every atomic natural charge in the group. These data indicate that the cyanine groups are donors and amide groups is acceptor and the charges were transferred through chemical bonds. The frontier molecular orbitals (MO) energies and corresponding density of state of the dye 6A2MP Dye is shown in Fig. 6.2 The HOMO–LUMO gap of the 6A2MP Dye in vacuum is 5.09 eV.

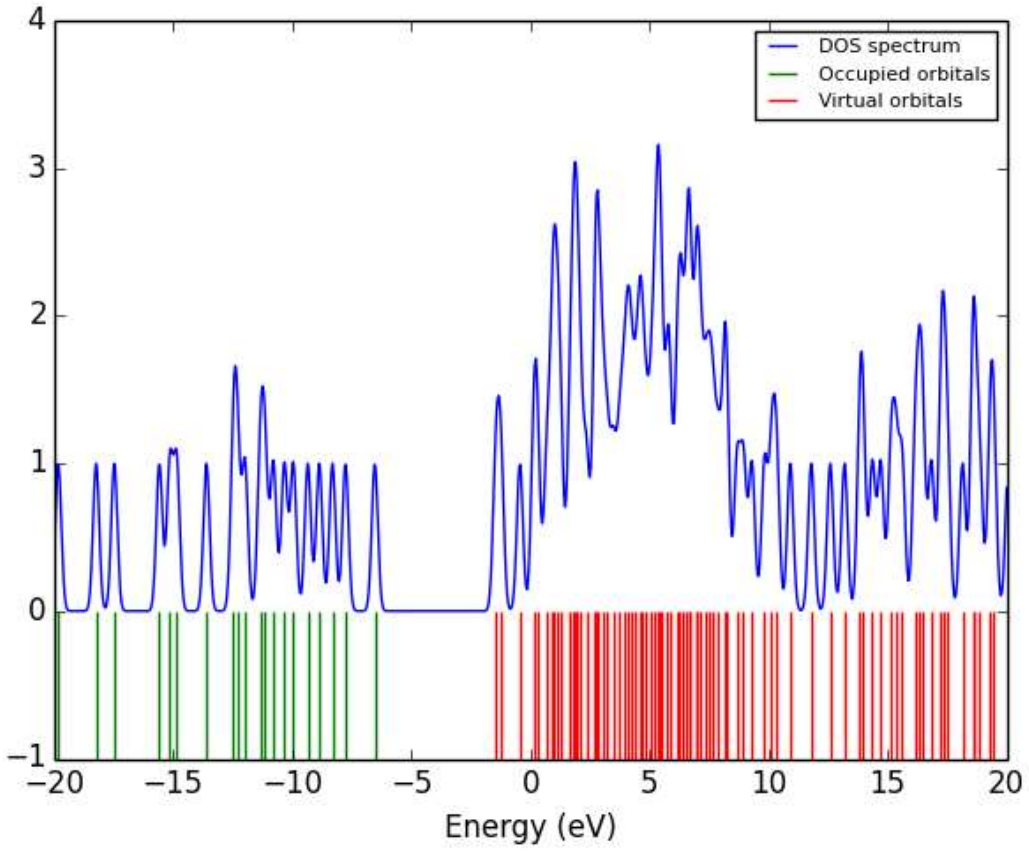

Fig.6.2 The frontier molecular orbital energies and corresponding DOS spectrum of the dye 6A2MP

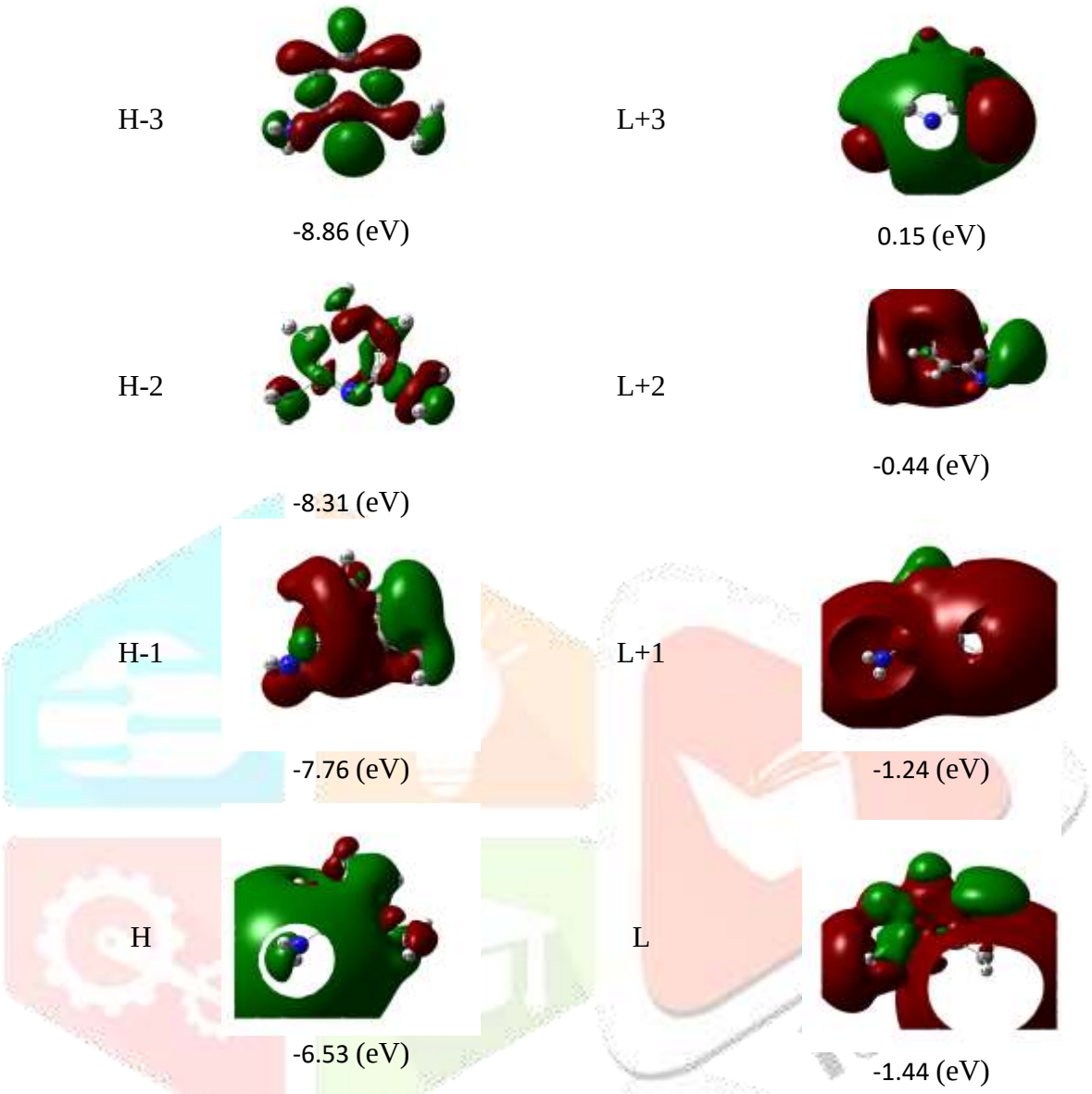

Fig. 6.3. Isodensity plots (isodensity contour = 0.02 a.u.) of the frontier orbitals of 6A2MP.

While the calculated HOMO and LUMO energies of the bare $Ti_{38}O_{76}$ cluster as a model for nanocrystalline are -6.55 and -2.77eV, respectively, resulting in a HOMO–LUMO gap of 3.78 eV, the lowest transition is reduced to 3.20 eV according to TDDFT, and this value is slightly smaller than typical band gap of TiO_2 nanoparticles with nm size [32]. Furthermore, the HOMO, LUMO and HOMO–LUMO gap of $(TiO_2)_{60}$ cluster is -7.52, -2.97, and 4.55 eV (B3LYP/VDZ), respectively [33]. Taking into account of the cluster size effects and the calculated HOMO, LUMO, HOMO–LUMO gap of the dye 6A2MP Dye, $Ti_{38}O_{76}$ and $(TiO_2)_{60}$ clusters, we can find that the HOMO energies of these dyes fall within the TiO_2 gap.

The above data also reveal the interfacial electron transfer between semiconductor TiO_2 electrode and the dye sensitizer 6A2MP Dye is electron injection processes from excited dye to the semiconductor conduction band. This is a kind of typical interfacial electron transfer reaction [34].

4.3. IR and Raman frequencies

Fig6.3 and 6.4 shows the observed and calculated IR and Raman spectra of 6A2MP Dye respectively. Comparison of the observed (FT-IR and FT-Raman) and calculated vibrational frequencies of 6A2MP Dye is shown in Table 6.4. Comparison of the frequencies calculated by ab initio HF and B3LYP with experimental values reveals the overestimation of the calculated vibrational modes due to neglect of anharmonicity in real system. Inclusion of electron correlation in density functional theory to a certain extent makes the frequency values smaller in comparison with experimental values. Any way notwithstanding the level of calculations it is customary to scale down the calculated harmonic frequencies in order to improve the agreement with the experiment. In our study we have followed two different scaling factors B3LYP/6-311++G (d,p) and HF/6-311++G(d,p). The 6A2MP Dye molecule give rise to two C-H stretching, six C-H wagging vibrations, five C-H in-plane bending vibration, four wagging C-C-N vibrations,three C-C-N vibrations, one C-C-N stretching vibration, ten C=C stretching vibrations, two C-N stretching vibrations, three C-H stretching vibrations, three ring deformation vibrations and five overtone combination, one N-H Asssymetric stretching, two NH2 Symmetric stretching one NH2 Assymetric stretching, one NH Stretching. The strongest IR absorption is attributed to vibrational mode 38 near about 2815 cm^{-1}, corresponding to stretching mode of C- N stretching bonds. The next absorption for 6A2MP Dye corresponds to the vibrational mode 42 near about 3450 cm^{-1}, which is the N-H2 symmetric Stretching bonds. In the Raman spectra, however, the strongest activity mode is the vibrational mode 37 near about 2750 cm^{-1}, which is corresponding to N-H asymmetric stretching mode.

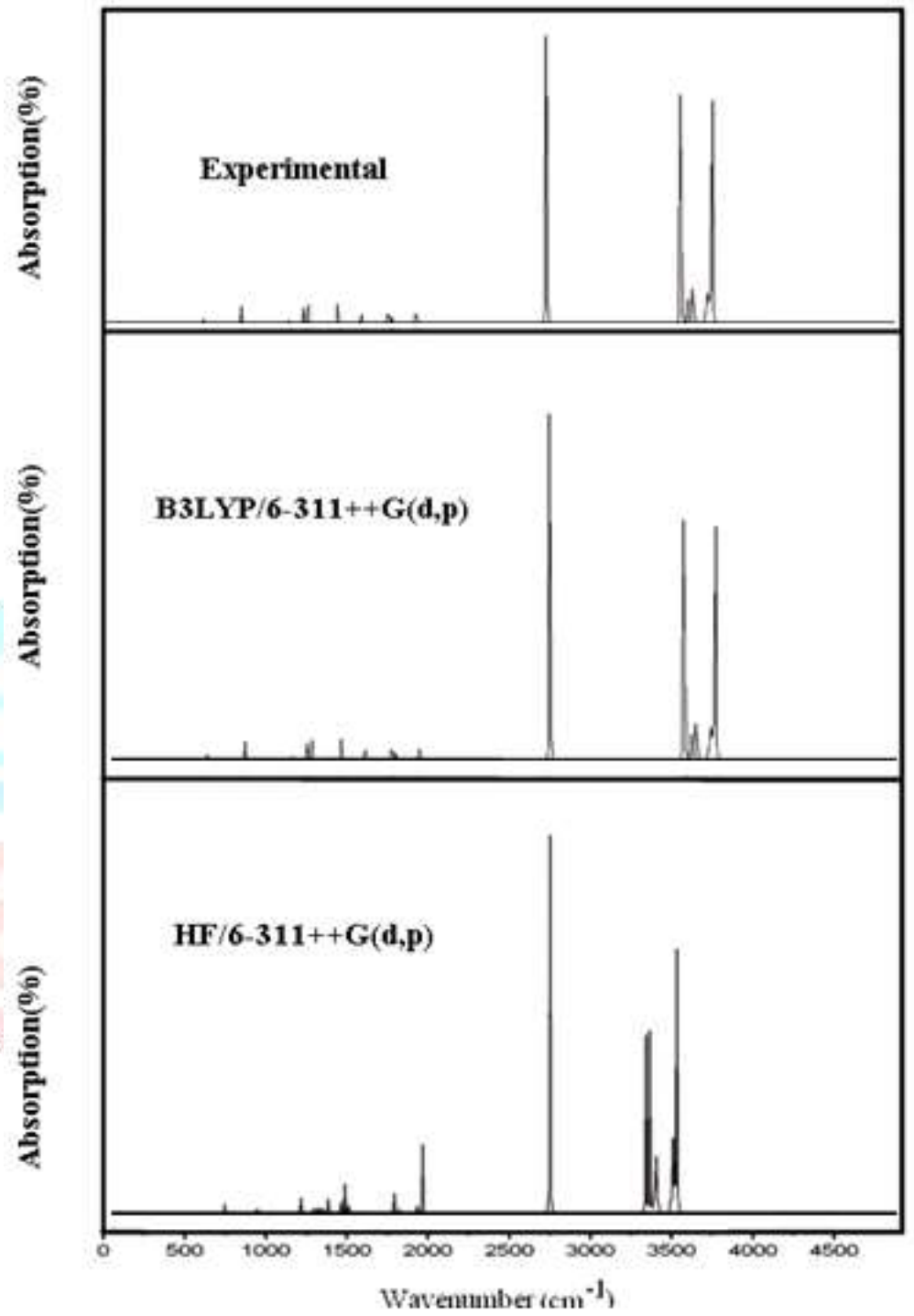

Fig. 6.4 Observed and Calculated FT-IR Spectra of 6A2MP

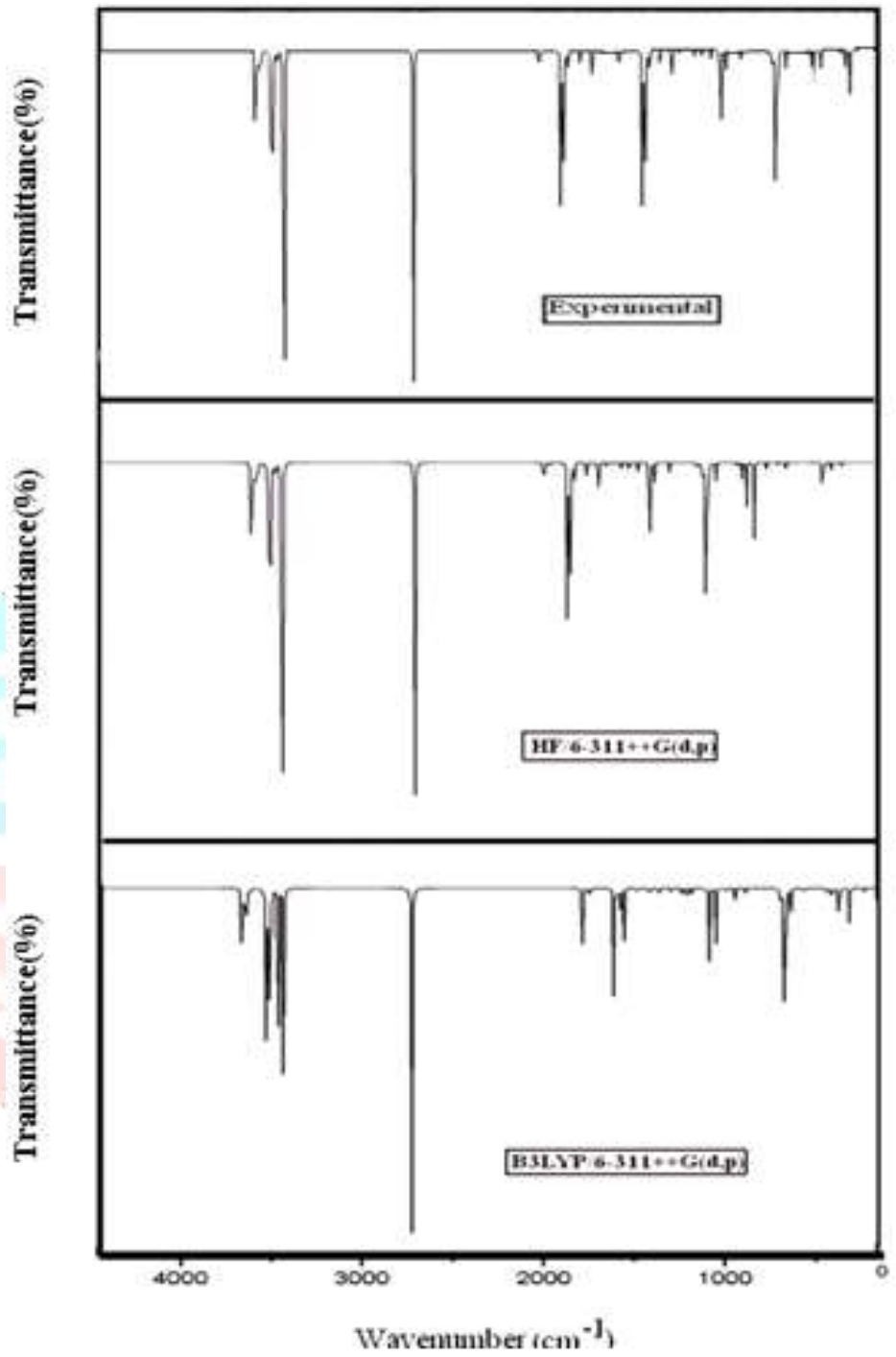

Fig. 6.5 Observed and Calculated FT-Raman Spectra of 6A2MP

Table 6.2 Comparison of the observed (FT-IR and FT-Raman) and calculated vibrational frequencies of 6A2MP

Vibrational mode no.	Species	Experimental		Scaled Wavenumber (cm^{-1})		IR Intensity	Raman active	Depolarisation Ratio	Reduced Mass	Force Constants	Assignments
		FT-IR	FT-Raman	HF/6-311G(d,p)	B3LYP/6-311G(d,p)						
1	A''	-	-	8.5726	27.9109	0.5079	0.4451	0.7421	1.0252	0.0005	C-C-N wagging
2	A'	-	-	101.6127	89.2051	1.0728	0.2801	0.7499	5.3814	0.0252	C-C-N in plane bending
3	A'	-	-	171.9475	147.0858	4.6916	3.2835	0.7374	6.9397	0.0885	C-C-N wagging
4	A'	250	-	223.0360	205.1285	1.9065	0.6765	0.7500	3.5696	0.0885	C-C-N wagging
5	A'	275		267.3705	245.0480	20.7185	0.0516	0.4631	5.5202	0.1953	Overtone/ combination
6	A'	-	-	326.1327	302.0580	2.7458	0.6648	0.1712	2.7212	0.1463	Overtone/ combination
7	A''	-	-	378.4560	313.8658	270.1847	3.3939	0.7390	1.2872	0.0747	Overtone/ combination
8	A''	-	-	455.2536	424.8998	8.3385	1.0503	0.4111	2.4787	0.2637	Overtone/ combination
9	A'	400	-	465.0560	432.6951	1.2010	1.8306	0.4131	3.2938	0.3633	Ring deformation
10	A'	-	-	477.8190	437.9824	0.6200	6.4765	0.4863	5.6007	0.6330	C-H stretching
11	A'	485	-	508.7199	473.3454	37.4067	1.0173	0.6135	1.3148	0.1736	Ring deformation
12	A'	-	-	477.8190	538.2109	1.4093	3.0651	0.6963	7.5207	1.2836	Ring deformation
13	A''	-	-	605.4205	548.9968	2.7873	7.7694	0.2527	5.1004	0.9057	C-C-N wagging + C-H wagging
14	A'	685	-	677.4741	623.3835	1.2499	2.4105	0.1633	6.1754	1.4139	C-C-N in plane bending
15	A'	-	680	693.5080	633.8593	2.0927	0.3542	0.7324	2.9869	0.7071	C-C-N in plane bending
16	A''	725	-	768.4625	725.5698	2.7177	2.7446	0.0966	5.7473	1.7827	C-H wagging
17	A''	-	845	787.9703	739.6722	0.8310	25.3664	0.0672	5.8246	1.8776	.C-H wagging
18	A'	-	-	837.7767	764.9579	0.6289	0.9501	0.6255	4.0483	1.3957	C-H wagging
19	A''	982	-	909.8525	827.3829	38.6347	0.1386	0.6563	1.7288	0.6973	C-H inplane bending
20	A''	1021	-	1015.2318	959.1517	1.7777	4.8751	0.0752	2.8608	1.5506	C-H wagging
21	A'	1082	-	102.5090	980.3688	0.7642	0.1191	0.6307	1.3237	0.7496	C-H wagging
22	A''	-	-	1108.8501	1008.6819	8.2685	6.2072	0.1493	1.5960	0.9568	Overtone/ combination
23	A'	1160	-	1155.0038	1055.1822	2.4817	0.1302	0.7486	1.5755	1.0335	C-H in plane bending
24	A'	-	-	1192.1034	1099.3101	3.8637	12.8176	0.3713	1.8900	1.3457	C-H in plane bending

25	A’	-	1230	1218.1695	1127.8482	22.4199	6.0007	0.2335	1.8555	1.3906	C-H in plane bending
26	A’	-	1270	1254.6685	1207.7478	1.0711	1.8754	0.6014	1.8979	1.6310	C-H in plane bending
27	A’	-	-	1313.0226	1258.3279	6.5649	39.8085	0.2034	2.6001	2.4257	C-C stretching
28	A’	-	-	1369.1933	1314.1664	5.4100	20.0942	0.2493	4.8905	4.9763	C-C stretching
29	A’	1450	1460	1462.0045	1366.8975	82.3393	12.6305	0.1124	2.7708	3.0502	C-C stretching
30	A’	1520	1530	1530.6407	1411.0700	6.0743	11.0854	0.2547	1.3352	1.5664	C=C stretching + C-C-N stretching
31	A’	-	-	1578.0199	1445.0437	64.3046	3.5654	0.7308	2.5245	3.1059	C=C stretching
32	A’	-	-	1598.4310	1475.1437	67.3457	6.4320	0.3538	1.8725	2.4007	C=C stretching
33	A’	1715	1780	1599.3412	1482.6280	11.1155	7.3045	0.7474	1.0525	1.3632	C=C stretching
34	A’	-	-	1634.0301	1504.0626	78.7384	23.8580	0.3010	1.9805	2.6397	C=C stretching
35	A’	1945	-	1746.7972	1588.9351	67.5256	5.7953	0.3026	4.8078	7.1518	C=C stretching
36	A’	-	1960	1775.5931	1629.3987	25.2302	54.7680	0.5906	2.2181	3.4696	C≡N ,C–C≡N
37	A’	2080	2750	1795.2441	1648.9194	578.4908	91.2300	0.4963	2.1621	3.4635	N- H asym. Stretch C=C stretching
38	A’	2815	-	2562.6859	2316.9529	100.8909	621.9819	0.2975	12.6694	40.0720	C-N stretching
39	A’	-	-	3187.8718	3035.9294	5.0596	188.7759	0.0355	1.0387	5.6403	N H asym. Stretch C-N stretching
40		-	-	3246.2890	3086.5964	6.9674	62.2187	0.7367	1.0989	6.1683	C-H stretching
41		-	-	3285.2363	3142.1232	7.2740	53.2738	0.6684	1.1007	6.4029	NH2 symmetric stretching
42		3450	-	3341.8291	3179.7488	5.6774	82.3528	0.5474	1.0887	6.4856	NH2 symmetric stretching
43		3580	3600	3942.3781	3197.1254	4.6671	136.1714	0.1810	1.0963	6.6026	NH2 Asymmetric stretching
44		3660	3650	3818.9063	3596.7100	91.5226	252.0228	0.1543	1.0459	7.9716	C-H stretching
45		-	3780	3942.3781	3719.7626	44.1228	62.3340	0.7127	1.1034	8.9955	N-H stretching

4.4 Polarizability and Hyperpolarizability

Polarizabilities and hyperpolarizabilities characterize the response of a system in an applied electric field [35]. They determine not only the strength of molecular interactions (long-range intermolecular induction, dispersion forces, etc.) as well as the cross sections of different scattering and collision processes, but also the nonlinear optical properties (NLO) of the system [36, 37]. It has been found that the dye sensitizer hemicyanine system, which has high NLO property, usually possesses high photoelectric conversion performance [38]. In order to investigate the relationships among photocurrent generation, molecular structures and NLO, the polarizabilities and hyperpolarizabilities of 6A2MP Dye was calculated.

Table 6.3 Polarizability (α) of the dye 6A2MP (in a.u.).

α_{xx}	α_{xy}	α_{yy}	α_{xz}	α_{yz}	α_{zz}	α	$\Delta\alpha$
-64.2896	6.9995	-53.4287	2.4813	-0.0475	-61.0198	59.5793	9.6507

Table 6.4 Hyperpolarizability (β) of the dye 6A2MP (in a.u.).

β_{xxx}	β_{xxy}	β_{xyy}	β_{yyy}	β_{xxz}	β_{xyz}	β_{yyz}	β_{xzz}	β_{yzz}	β_{zzz}	β_{ii}
-141.3153	13.7060	-7.9655	-5.1620	-8.0429	0.4001	0.3992	1.5310	3.3275	0.4257	13.0421

The polarizabilities and hyperpolarizabilities could be computed via finite field (FF) method, sum-over state (SOS) method based on TDDFT, and coupled-perturbed HF (CPHF) method. However, the use of FF, SOS, and CPHF methods with large sized basis sets for 6A2MP Dye is too expensive. Here, the polarizability and the first hyperpolarizabilities are computed as a numerical derivative of the dipole moment using B3LYP/6-311++G(d,p). The definitions [36, 37] for the isotropic polarizability is refer eq 2.1, 2.2 and 2.3

Tables 6.2 and6.3 list the values of the polarizabilities and hyperpolarizabilities of the dye 6A2MP Dye. In addition to the individual tensor components of the polarizabilties and the first hyperpolarizabilities, the isotropic polarizability, polarizability anisotropy invariant and hyperpolarizability are also calculated. The calculated isotropic polarizability of 6A2MP Dye is 9.65 a.u. However, the calculated isotropic polarizability of JK16, JK17, dye 1, dye 2, D5, DST and DSS is 759.9, 1015.5, 694.7, 785.7, 510.6, 611.2 and 802.9 a.u., respectively [39,40]. The above data indicate that the donor-conjugate p bridge-acceptor (D-p-A) chain-like dyes have stronger response for external electric field. Whereas, for dye sensitizers D5, DST, DSS, JK16, JK17, dye 1 and dye 2, on the basis of the published photo-to-current conversion efficiencies, the similarity and the difference of geometries, and the calculated isotropic polarizabilities, it is found that the longer the length of the conjugate bridge in similar dyes, the larger the polarizability of the

dye molecule, and the lower the photo-to-current conversion efficiency. This may be due to the fact that the longer conjugate-p-bridge enlarged the delocalization of electrons, thus it enhanced the response of the external field, but the enlarged delocalization may be not favorable to generate charge separated state effectively. So it induces the lower photo-to-current conversion efficiency.

4.5. Electronic Absorption Spectra and Sensitized Mechanism

In order to understand the electronic transitions of 6A2MP Dye TD-DFT calculations on electronic absorption spectra in vacuum and solvent were performed, and the results are shown in Fig.6.5. It is observed that, for 6A2MP Dye, the absorption in the visible region is much weaker than that in the UV region. The calculated results have a red-shift. The results of TD-DFT have an appreciable red-shift, and the degree of red-shift in solvent is more significant than that in vacuum. The discrepancy between vacuum and solvent effects in TD-DFT calculations may result from two aspects. The first aspect is smaller gap of materials which induces smaller excited energies. The other is solvent effects. Experimental measurements of electronic absorptions are usually performed in solution. Solvent, especially polar solvent, could affect the geometry and electronic structure as well as the properties of molecules through the long-range interaction between solute molecule and solvent molecule. For these reasons it is more difficult to make the TD-DFT calculation is consistent with quantitatively. Though the discrepancy exists, the TD-DFT calculations are capable of describing the spectral features of 6A2MP Dye because of the agreement of line shape and relative strength as compared with the vacuum and solvent.

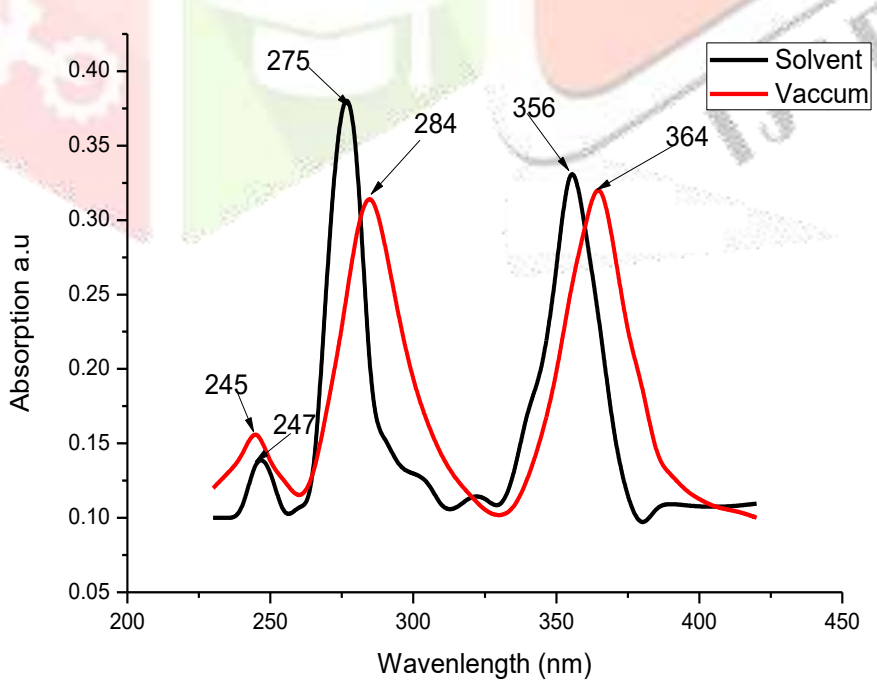

Fig. 6.6. Calculated electronic absorption spectra of the dye 6A2MP

The HOMO-LUMO gap of 6A2MP Dye in acetonitrile at B3LYP/6-311++G (d,p) theory level is smaller than that in vacuum. This fact indicates that the solvent effects stabilize the frontier orbitals of 6A2MP Dye. So it induces the smaller intensities and red-shift of the absorption as compared with that in vacuum.

In order to obtain the microscopic information about the electronic transitions, the corresponding MO properties are checked. The absorption in visible and near-UV region is the most important region for photo-to-current conversion, so only the 20 lowest singlet/singlet transitions of the absorption band in visible and near-UV region for 6A2MP Dye is listed in Table 6.4. The data of Table 4 and Fig.6 are based on the 6-311++G (d, p) results with solvent effects involved.

Table 6.5 Computed excitation energies, electronic transition configurations and oscillator strengths (f) for the optical transitions with f > 0.01 of the absorption bands in visible and near- UV region for the 6A2MP dye in acetonitrile.

State	Excitation energy (eV)	Wavelength (nm)	Major transitions corresponding orbital's
1	4.5764	364	HOMO->LUMO (95%)
2	4.9220	360	H-1->LUMO (85%)
3	5.0236	355	HOMO->L+1 (80%)
4	5.0546	351	H-2->LUMO (90%)
5	5.2586	348	H-1->L+1 (98%)
6	5.4557	340	H-8->LUMO (79%)
7	5.7201	339	H-3->LUMO (10%), H-1->L+2 (11%), HOMO->L+2 (60%)
8	5.8360	336	H-4->LUMO (11%), H-3->LUMO (68%), H-1->L+1 (10%)
9	6.0861	332	H-4->LUMO (73%), HOMO->L+2 (10%)
10	6.1080	328	H-5->LUMO (82%)
11	6.2236	323	H-6->LUMO (19%), H-1->L+2 (56%)
12	6.3530	319	H-6->LUMO (73%), H-1->L+2 (12%)
13	6.4116	315	H-1->L+3 (34%), HOMO->L+3 (61%)
14	6.4680	300	H-2->L+1 (25%), H-1->L+4 (16%), HOMO->L+4 (43%)
15	6.5462	295	H-2->L+1 (59%), H-1->L+4 (12%), HOMO->L+4 (18%)
16	6.5924	291	H-7->LUMO (79%)
17	6.7647	284	H-3->L+1 (66%)
18	6.7961	270	H-1->L+3 (44%), HOMO->L+3 (30%)

19	6.8658	264	H-4->L+1 (39%), HOMO->L+5 (16%)
20	6.9684	245	H-4->L+1 (30%), H-2->L+2 (15%)

Where I_0 is the photon flux, *Jsc* is the short-circuit photocurrent density, and *Voc* is the open-circuit photovoltage, and ff represents the fill factor [41]. At present, the *Jsc*, the *Voc*, and the *ff* are only obtained by experiment, the relationship among these quantities and the electronic structure of dye is still unknown. The analytical relationship between Voc and E_{LUMO} may exist. According to the sensitized mechanism (electron injected fr This indicates that the transitions are photoinduced charge transfer processes, thus the excitations generate charge separated states, which should favour the electron injection from the excited dye to semiconductor surface.

The solar energy to electricity conversion efficiency (η) under AM 1.5 white-light irradiation can be obtained from the following formula: refer eq. (2.4)

on the excited dyes to the semiconductor conduction band) and single electron and single state approximation, there is an energy relationship: refer eq. (2.5)

Where, E_{CB} is the energy of the semiconductor's conduction band edge. So the Voc may be obtained applying the following formula: refer eq. (2.6)

It induces that the higher the E_{LUMO}, the larger the V_{oc}. The results of organic dye sensitizer JK16 and JK17 [39], D-ST and D-SS also proved the tendency [42] (JK16:LUMO = -2.73 eV, V_{oc} = 0.74 V; JK17: LUMO = -2.87 eV, V_{oc} = 0.67 V; D-SS: LUMO = -2.91 eV, V_{oc} = 0.70 V; D-ST: LUMO = -2.83 eV, V_{oc} = 0.73 V). Certainly, this formula expects further test by experiment and theoretical calculation**.** The J_{sc} is determined by two processes, one is the rate of electron injection from the excited dyes to the conduction band of semiconductor, and the other is the rate of redox between the excited dyes and electrolyte. Electrolyte effect on the redox processes is very complex, and it is not taken into account in the present calculations. This indicates that most of excited states of 6A2MP Dye have larger absorption coefficient, and then with shorter lifetime for the excited states, so it results in the higher electron injection rate which leads to the larger Jsc of 6A2MP Dye. On the basis of above analysis, it is clear that the 6A2MP Dye has better performance in DSSC.

5. Conclusion

The geometries, electronic structures, polarizabilities, and hyperpolarizabilities of dye 6A2MP was studied by using ab initio HF and DFT with hybrid functional B3LYP, and the UV-Vis spectra were investigated by using TD-DFT methods. The NBO results suggest that 6A2MP Dye is a (D-π-A) system. The calculated isotropic polarizability of 6A2MP Dye is 9.65 a.u. The calculated polarizability anisotropy invariant of 6A2MP Dye is 59.57 a.u. The hyperpolarizability of 6A2MP Dye is 13.042 (in a.u). The

strongest IR absorption is attributed to vibrational mode 38 near about 2815 cm^{-1}, corresponding to stretching mode of C- N stretching bonds. The next absorption for 6A2MP Dye corresponds to the vibrational mode 42 near about 3450 cm^{-1}, which is the N-H2 symmetric Stretching bonds. In the Raman spectra, however, the strongest activity mode is the vibrational mode 37 near about 2750 cm^{-1}, which is corresponding to N-H asymmetric stretching mode.

The electronic absorption spectral features in visible and near-UV region were assigned based on the qualitative agreement to TD-DFT calculations. The absorptions are all ascribed to $\pi \rightarrow \pi^*$ transition. The three excited states with the lowest excited energies of 6A2MP Dye is photo induced electron transfer processes that contribute sensitization of photo-to-current conversion processes. The interfacial electron transfer between semiconductor TiO_2 electrode and dye sensitizer 6A2MP Dye is electron injection process from excited dye as donor to the semiconductor conduction band. Based on the analysis of geometries, electronic structures, and spectrum properties between 6A2MP Dye the role of cyanine and amine group is as follows: it enlarged the distance between electron donor group and semiconductor surface, and decreased the timescale of the electron injection rate, resulted in giving lower conversion efficiency. This indicates that the choice of the appropriate conjugate bridge in dye sensitizer is very important to improve the performance of DSSC.

References

[1] B. O'Regan, M. Gratzel, Nature 353 (1991) 737-739.

[2] M. Gratzel, Nature 414 (2001) 338-344.

[3] N.G. Park, K. Kim, Phys. Status Solidi a. 205 (2008) 1895-1904.

[4] Y. Chiba, A. Islam, Y. Watanabe, R. Komiya, N. Koide, L. Han, Jpn. J. Appl. Phys 45 (2006) L638-L640.

[5] K. Hara, M. Kurashige, Y. Dan-oh, C. Kasada, A. Shinpo, S. Suga, K. Sayama, H. Arakawa, New J. Chem. 27 (2003) 783-785.

[6] T. Kitamura, M. Ikeda, K. Shigaki, T. Inoue, N. A. Anderson, X. Ai, T. Lian, S. Yanagida, Chem. Mater. 16 (2004) 1806-1812.

[7] T. Horiuchi, H. Miura, K. Sumioka, S. Uchida, J. Am. Chem. Soc. 126 (2004) 12218-12219.

[8] W. M. Campbell, A. K. Burrell, D. L. Officer, K. W. Jolley, Coord. Chem. ReV. 248 (2004) 1363-1379.

[9] K. R. J. Thomas, J. T. Lin, Y. C. Hsu, K. C. Ho, Chem. Commun. (2005) 4098-4100.

[10] D. P. Hagberg, T. Edvinsson, T. Marinado, G. Boschloo, A. Hagfeldt, L. Sun, Chem. Commun. (2006) 2245-2247.

[11] S. L. Li, K. J. Jiang, K. F. Shao, L. M. Yang, Chem. Commun. (2006) 2792-2794.

[12] N. Koumura, Z. S.Wang, S. Mori, M. Miyashita, E. Suzuki, K. Hara, J. Am. Chem. Soc. 128 (2006) 14256-14257.

[13] S. Kim, J. W. Lee, S. O. Kang, J. Ko, J. H. Yum, S. Fantacci, F. De Angellis, D. Di Censo, M. K. Nazeeruddin, M. J. Gratzel, Am. Chem. Soc., 128 (2006) 16701-16707.

[14] Z. S. Wang, Y. Cui, K. Hara, Y. Dan-oh, C. Kasada, A. Shinpo, AdV. Mater., 19 (2007) 1138-1141.

[15] T. Edvinsson, C. Li, N. Pschirer, J. Schoneboom, F. Eickemeyer, R. Sens, G. Boschloo, A. Herrmann, K. Mullen, A. Hagfeldt, J. Phys. Chem. C 111 (2007) 15137-15140.

[16] M. Wang, M. Xu, D. Shi, R. Li, F. Gao, G. Zhang, Z. Yi, R. Humphry-Baker, P. Wang, S. M. Zakeeruddin, M. Gratzel, AdV. Mater., 20 (2008) 4460-4463.

[17] D. Shi, N. Pootrakuchote, Z. Yi, M. Xu, S. M. Zakeeruddin, M. Gratzel, P. J. Wang, Phys. Chem. C, 112 (2008) 17478-17484.

[18] G. Zhou, N. Pschirer, J. C. Schoneboom, F. Eickemeyer, M. Baumgarten, K. Mullen, Chem. Mater., 20 (2008) 1808-1815.

[19] J. T. Lin, P. C. Chen, Y. S. Yen, Y. C. Hsu, H. H. Chou, M. C. P. Yeh, Org. Lett., 11 (2009) 97-100.

[20] G. Zhang, Y. Bai, R. Li, D. Shi, S. Wenger, S. M. Zakeeruddin, M. Gratzel, P. Wang, Energy Environs. Sci., 2 (2009) 92-95.

[21] M. Xu, S. Wenger, H. Bara, D. Shi, R. Li, Y. Zhou, S. M. Zakeeruddin, M. Gratzel, P. Wang, J. Phys. Chem. C, 113 (2009) 2966-2973.

[22] X.H. Zhang, C. Li, W.B. Wang, X.X. Cheng, X.S. Wang, B.W. Zhang, J. Mater.Chem. 17 (2007) 642-649.

[23] M. Liang, W. Xu, F. Cai, P. Chen, B. Peng, J. Chen, Z. Li, J. Phys. Chem. C, 111 (2007) 4465-4472.

[24] W. Xu, B. Peng, J. Chen, M. Liang, F. Cai, J. Phys. Chem. C, 112 (2008) 874-880.

[25] S. Ito, H. Miura, S. Uchida, M. Takata, K. Sumioka, P. Liska, P. Comte, P. Pechy, M. Gratzel, Chem. Commun. (2008) 5194-5196.

[26] M.J. Frisch, G.W. Trucks, H.B. Schlegel, G.E. Scuseria, M.A. Robb, J.R. Cheeseman, J.A. Montgomery Jr., T. Vreven, K.N. Kudin, J.C. Burant, J.M. Millam, S.S. Iyengar, J. Tomasi, V. Barone, B. Mennucci, M. Cossi, G. Scalmani, N. Rega, G.A. Petersson, H. Nakatsuji, M. Hada, M. Ehara, K. Toyota, R. Fukuda, J. Hasegawa, M. Ishida, T. Nakajima, Y. Honda, O. Kitao, H. Nakai, M. Klene, X. Li, J.E. Knox, H.P. Hratchian, J.B. Cross, C. Adamo, J. Jaramillo, R. Gomperts, R.E. Stratmann, O. Yazyev, A.J. Austin, R. Cammi, C. Pomelli, J.W. Ochterski, P.Y. Ayala, K. Morokuma, G.A. Voth, P. Salvador, J.J. Dannenberg, V.G. Zakrzewski, S.Dapprich, A.D. Daniels, M.C. Strain, O. Farkas, D.K. Malick, A.D. Rabuck, K. Raghavachari, J.B. Foresman, J.V. Ortiz, Q. Cui, A.G. Baboul, S. Clifford, J.Cioslowski, B.B. Stefanov, G. Liu, A. Liashenko, P. Piskorz, I. Komaromi, R.L. Martin, D.J. Fox, T. Keith, M.A. Al-Laham, C.Y. Peng, A. Nanayakkara, M. Challacombe, P.M.W. Gill, B. Johnson, W. Chen, M.W. Wong, C. Gonzalez, J.A. Pople, Gaussian 09, Gaussian, Inc., Pittsburgh, PA, 2009.

[27] A.D. Becke, J. Chem. Phys. 98 (1993) 5648-5652.

[28] B. Miehlich, A. Savin, H. Stoll, H. Preuss, Chem. Phys. Lett. 157 (1989) 200-206.

[29] C. Lee, W. Yang, R.G. Parr, Phys. Rev. B. 37 (1988) 785-789.

[30] V. Barone, M. Cossi, J. Phys. Chem. A, 102 (1998) 1995-2001.

[31] M. Cossi, N. Rega, G. Scalmani, V. Barone, J. Comput. Chem. 24 (2003) 669-681.

[32] M.K. Nazeeruddin, F. De Angelis, S. Fantacci, A. Selloni, G. Viscardi, P. Liska, S.Ito, B. Takeru, M. Gratzel, J. Am. Chem. Soc. 127 (2005) 16835-16847.

[33] M.J. Lundqvist, M. Nilsing, P. Persson, S. Lunell, Int. J. Quantum Chem. 106 (2006) 3214-3234.

[34] D.F. Waston, G.J. Meyer, Annu. Rev. Phys. Chem. 56 (2005) 119-156.

[35] C. R. Zhang, H. S. Chen, and G. H. Wang, Chem. Res. Chin. U. 20 (2004) 640-646.

[36] Y. Sun, X. Chen, L. Sun, X. Guo, W. Lu, Chem.Phys. Lett. 381 (2003) 397-403.

[37] O. Christiansen, J. Gauss, J. F. Stanton, Chem.Phys. Lett. 305 (1999) 147-155.

[38] Z. S. Wang, Y. Y. Huang, C. H. Huang, J. Zheng, H.M. Cheng, S. J. Tian, Synth. Met. 14 (2000) 201-207.

[39] C.R. Zhang, Y.Z. Wu, Y.H. Chen, H.S. Chen, Acta Phys. Chim. Sin. 25 (2009) 53-60.

[40] A. Seidl, A. Gorling, P. Vogl, J. A. Majewski, M. Levy, Phys. Rev. B 53 (1996) 3764-3774.

[41] K. Hara, T. Sato, R. Katoh, A. Furube, Y. Ohga, A. Shinpo, S. Suga, K. Sayama, H.Sugihara, H. Arakawa, J. Phys. Chem. B. 107 (2003) 597-606.

[42] C.R. Zhang, Z.J. Liu, Y.H. Chen, H.S. Chen, Y.Z. Wu, L.H. Yuan, J. Mol. Struct. (THEOCHEM) 899 (2009) 86-93.